Microstructural Characterization of Thin Film Photovoltaics using Electron Backscatter Diffraction

Matthew M. Nowell, *EDAX-TSL*

Summary

- The demand for alternative sources of energy is expected to continue to grow.
- Photovoltaic thin film solar cells provide a commercially viable technology that can capture increased power generation market share.
- Polycrystalline CdTe and CIGS thin films have higher efficiencies than single crystal devices.
- The performance of these thin films is influenced by the crystallographic structure, grain boundary character, and grain size.
- EDAX's Orientation Imaging Microscopy (OIM) is a market-leading analytical technique capable of measuring all of these factors simultaneously with sub-micron resolution.
- OIM also has unique capabilities of characterizing Twin Boundaries.

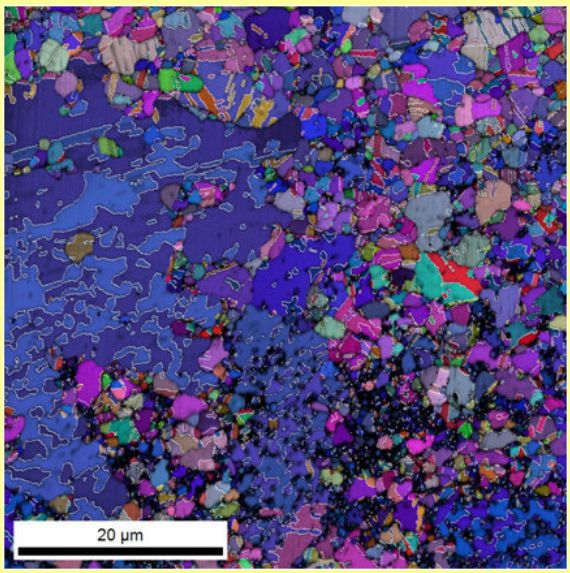

This image shows an orientation map from a CdTe photovoltaic thin film. The white lines indicate twin boundaries, which exhibit superior electrical properties than random high-angle grain boundaries. 45% of the boundaries are twin boundaries.

Introduction

Worldwide demand for electricity is growing and the driving force to develop new technologies and materials for alternative energy generation has been increasing due to economic, environmental, and political factors in recent years. Solar power is one such alternative being investigated through photovoltaic (PV) materials that convert sunlight into useable electrical energy. PV production has demonstrated significant growth rates, and this growth is expected to continue.

The majority of traditional solar cells are based on crystalline silicon. However the cost of this technology is still too high to compete with other means of power generation. One of the largest contributors to this cost is the silicon wafer used. Thin film photovoltaics are an alternative which use less material than traditional silicon solar cells and can be fabricated on a variety of lower cost substrates, including flexible low-mass and thin foil substrates that allow for potential new applications.

Two promising thin film materials are based on Cadmium Telluride (CdTe) and chalcopyrite-structured materials such as $Cu(In,Ga)Se_2$ (CIGS). These materials have near-optimal band gaps, high optical absorption, and good conversion efficiencies. Solar modules manufactured from these materials are commercially available. However the efficiencies of the commercial

modules are lower than research-grade cells, indicating an area of potential improvement. Additionally these materials exhibit an unexpected characteristic. Both CdTe and CIGS devices are fabricated as polycrystalline thin films. Surprisingly these devices have higher efficiencies than their single-crystal counterparts, in direct contrast to Silicon and Gallium Arsenic (GaAs) devices [1]. This difference most likely arises from the role grain boundaries play in these materials.

Grain Boundaries

The grain boundaries present in polycrystalline materials are defects within the crystalline lattice that are expected to reduce photovoltaic performance through increased recombination rates. Grain boundaries can also act as localized accumulation sites for defect collection, which can lead to an improvement in crystal lattice quality within the interior of the grains and better photoelectric performance. Both structural and electronic grain boundary models have been proposed to explain the improved performance of these polycrystalline thin films materials. At the grain boundaries, periodicity of the atomic lattice is disrupted, free surface-like conditions occur, and the boundaries can become preferred sites for chemical diffusion and segregation. This can lead to the development of trapped localized electrical or polar charges that cause a region of depleted majority carriers (holes) in the vicinity of grain boundaries and a potential barrier for majority carrier transport. This condition has been verified with a variety of analytical techniques such as scanning capacitance microscopy (SCM) [2], scanning Kelvin probe microscopy (SKPM) [3], conductive probe atomic force microscopy (CP-AFM), and electron beam and ion beam induced current (EBIC and IBIC) [4] and cathodoluminescence (CL) imaging [5]. While majority carrier transport and photovoltaic-induced current is reduced in these regions, the presence of the depleted regions adjacent to grain boundaries can improve the separation and collection and recombination behavior of both majority and minority carriers, with holes flowing in one direction through the grain interiors and electrons flowing the other direction within grain boundaries.

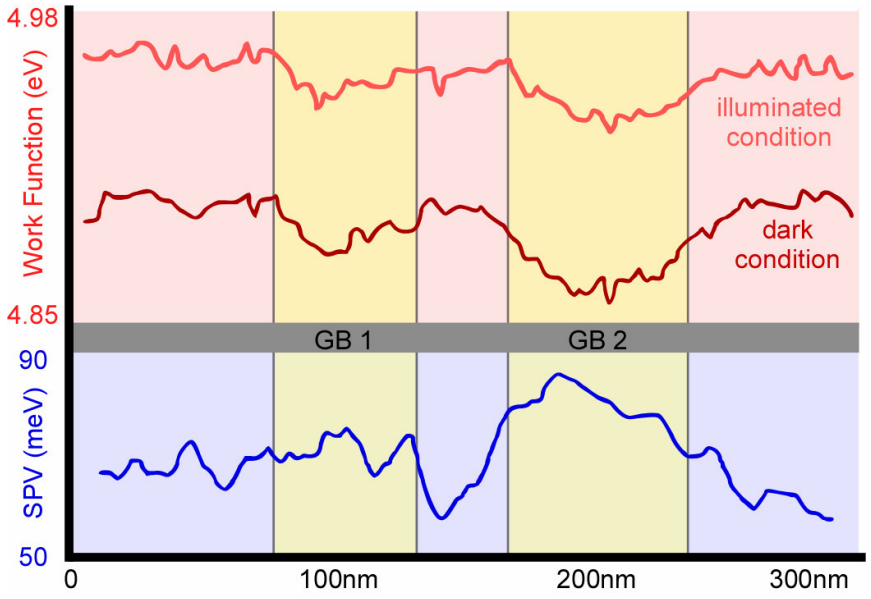

Figure 1 - Work function measurements on CGS film using Kelvin Probe Force Microscopy (red). The surface photovoltage (SPV) distribution is also shown (blue). Different grain boundary types are inferred from the differences in SPV behavior. Adapted from [6] with permission.

However not all grain boundaries are equal. Measurements of photoelectric behavior on individual grain boundaries show variations. Figure 1 shows work function measurements collected with KPFM across two grain boundaries in a $CuGaSe_2$ (CGS) film (Adapted from Marrón et. al. [6] with permission). The red curves show the work functions under illumination and dark conditions. The blue curve shows the surface photovoltage (SPV) distribution. These two boundaries exhibit different SPV character, which suggest different types of grain

boundaries. One type of grain boundary is a twin boundary, which can be described in terms of a coincident site lattice (CSL) model [7]. CSL boundaries describe orientation relationships where there is improved fit between adjacent grains, which can result in more complete bonding relative to a random grain boundary. This can lower grain boundary energy, and result in different electrical, diffusional, segregation, and transport properties. Twin boundaries are often referred to as Σ3 CSL boundaries. For example, differences between Σ3 twin boundaries and random boundaries in CIGS films have been observed with CL imaging [5]. Absolute values of CSL boundary properties vary between CdTe and CIGS films due to the difference in crystal structure, however the relative trends in electrical properties are still present [8].

Similar results have been shown with EBIC and IBIC [4]. In these measurements, induced current variations are seen at different grain boundaries. In addition, non-uniform response is observed between different grains, which could be related to the crystallographic orientation. Figure 2 shows an EBIC current map under high beam current illumination (Adapted from Baier et. al. [4] with permission). Not only are grain and grain boundary variations present, but the response near the grain boundary in one grain is affected by the current value of the adjacent grain as well. This suggests that both grain orientation and grain boundary structure details affect photovoltaic behavior. For example, high efficiency (18.8%) CIGS cells exhibited a (220)/(204) preferred orientation [9].

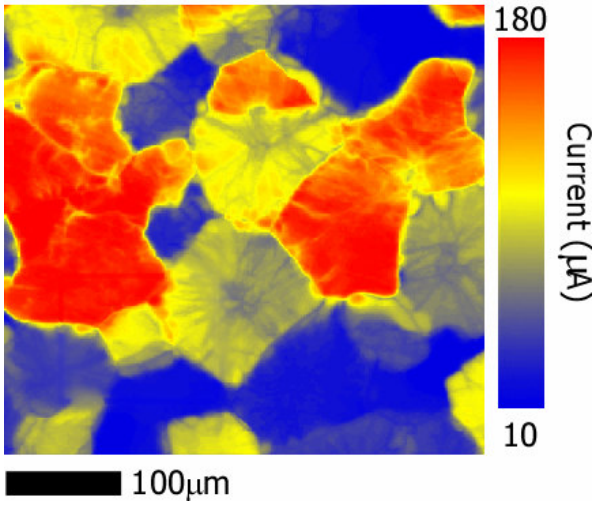

Figure 2 - Electron Beam Induced Current image taken at 53.5nA current illumination of CdTe film with a sample bias of 100V. Adapted from [4] with permission.

Figure 3 shows KPFM results from a CGS film where the relationship between local work function and crystallographic orientation has been identified (Adapter from Sadewasser et. al. [3] with permission). In this case, measurements were taken from a single grain of known orientation, and the facet surface orientations identified by measuring the angles between facets. Facets of similar orientation exhibit similar work functions, suggesting that the surface atomic configuration as defined by the crystallographic orientation helps determine the localized work function.

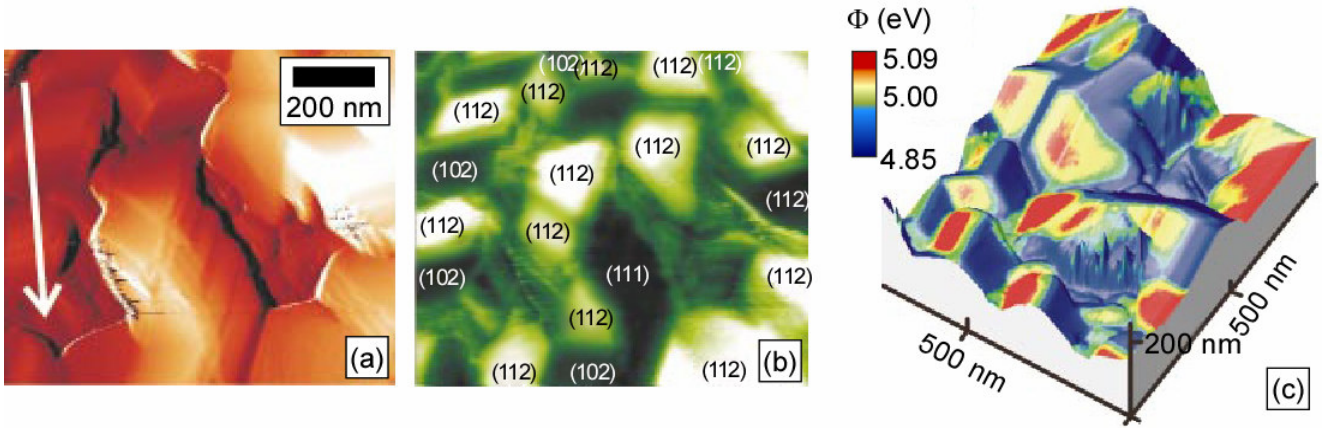

Figure 3 - Kelvin Probe Force Microscopy measurement of a CGS film showing (a) topographic image with facets. (b) Representation of the measured work function with crystallographic facets labeled. (c) 3D image combining topography and work function measurements. Adapted from [3] with permission.

The concept that grain boundaries, and different grain boundary types, can have both advantageous and adverse effects in solar cells is not new, nor the idea to engineer devices to increase the fraction of preferred boundaries [10]. This idea is related to the concept of measuring third level metrics (3LM), or the underlying microstructural features that govern film performance [11, 12]. Traditionally it has been difficult to measure the crystallographic grain boundary character of a material and therefore to correlate electrical properties with specific grain boundary structures. Transmission Electron Microscopy (TEM) has been used to characterize grain boundaries, but is limited by extensive sample preparation and the limited number of boundaries typically observed. X-Ray Diffraction does not measure crystallographic information in a spatially-specific manner required to resolve grain boundary information, but does provide information on preferred orientation, or texture. Electron Channeling Patterns (ECP) in a Scanning Electron Microscope (SEM) does not provide the necessary spatial resolution or automation for thin film measurements. A new analytical technique was required.

Electron Backscatter Diffraction (EBSD)

EBSD is an SEM-based characterization technique for measuring crystallographic orientation. An EBSD pattern from CdTe is shown in Figure 4. Information regarding orientation, phase, and strain can be extracted from these patterns. Orientation Imaging Microscopy (OIM) is the automated collection and analysis of EBSD patterns to create micrographs based on orientations and to quantitatively characterize the microstructure of a material.

EBSD patterns are generated from approximately a 5nm x 15nm x 15nm volume of material interacting with the electron beam and producing diffraction patterns that are imaged with a low light digital camera. As such, EBSD patterns are sensitive to surface defects and oxide layers that may be present within this interaction volume. Additionally, EBSD pattern detection requires a line-of-sight view from the detector. Surface topography may inhibit this view and decrease collection efficiency. Because of these issues, EBSD-specific sample preparation may be required [13]. For plan-view analysis, broad beam ion etching can be used to smooth the film surface. This can be done in conjunction with careful abrasive polishing as well. For cross-sectional analysis, mechanical polishing is typically required prior to ion milling. In either case, low energy (0.5-2.5 keV) ions typically produce the highest quality EBSD patterns. Cross-sections allow visualization of the microstructure relative to the direction of current flow. This may be important depending on the geometry of the grain boundaries. Plan-views typically allow for better collection statistics with more grains and grain boundaries observed.

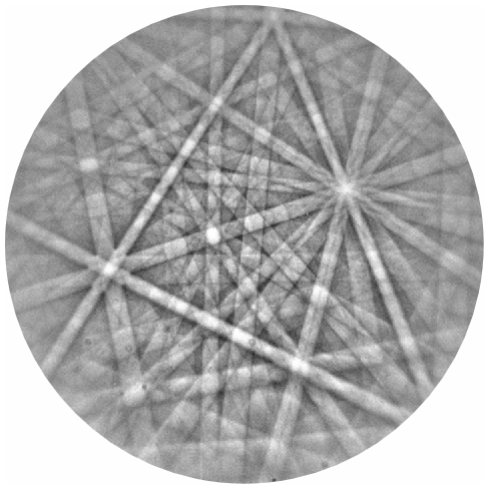

Figure 4 – EBSD pattern from CdTe thin film.

As CdTe and CIGS films are semiconductors, some care must be exercised to avoid charging and drift problems during OIM mapping. Appropriate selection of electron beam current and OIM acquisitions speeds are needed to avoid these problems. Typically, faster acquisition speeds are a good method as, in addition to avoiding localized charge effects, they also help counter stage drift and beam stability issues. Additionally a thin carbon coating applied to the film surface may improve conductivity without adversely effecting EBSD pattern quality.

CIGS films can present a challenge to EBSD as well. These materials have a tetragonal chalcopyrite structure, which exhibits cubic pseudo-symmetry. Careful analysis of the EBSD patterns is required in order to accurately determine the correct crystallographic orientation variant [14].

Case Study – $CdCl_2$ Treatment of CdTe Films

To help understand the microstructural effects of the commonly used $CdCl_2$ activation treatment on CdTe thin films, two treated samples were examined with OIM. The films studied were fabricated as CdTe/CdS/*i*-SnO_2/SnO_2/Glass, with the CdS deposited by chemical bath deposition and the CdTe was deposited by physical vapor deposition (PVD) at 325ºC with a CdTe film thickness of approximately 3µm. Samples were then treated at 350ºC with $CdCl_2$ vapor for either 5 or 30 minutes (Sample 1 and 2 respectively). This treatment is considered necessary to produce good CdTe films by passivating the grain boundaries with Cl [15]. This treatment is not necessary for CIGS films. $CdCl_2$ treated films exhibit stronger grain boundary depletion regions and significant core minority-driven currents [1]. Recombination efficiency also improves, with an example of 78% recombination prior to treatment and 38% after treatment [16].

To maximize OIM spatial resolution and minimize any adverse collection effects from surface roughness, the CdTe surfaces were prepared using an FEI Quanta 3D Dual Beam instrument. With this instrument, a focused Ga ion beam, operating at 30kV energy and 1nA of current, was used to cut a flat surface on the film. A glancing angle of 1.5º was used. As such, the surface plane analyzed started at the film surface and sampled into the depth of the film approximately 1.5µm. Figure 5 shows OIM orientation maps collected from these surfaces from samples 1 and 2, with the film surface level located at the bottom of each map.

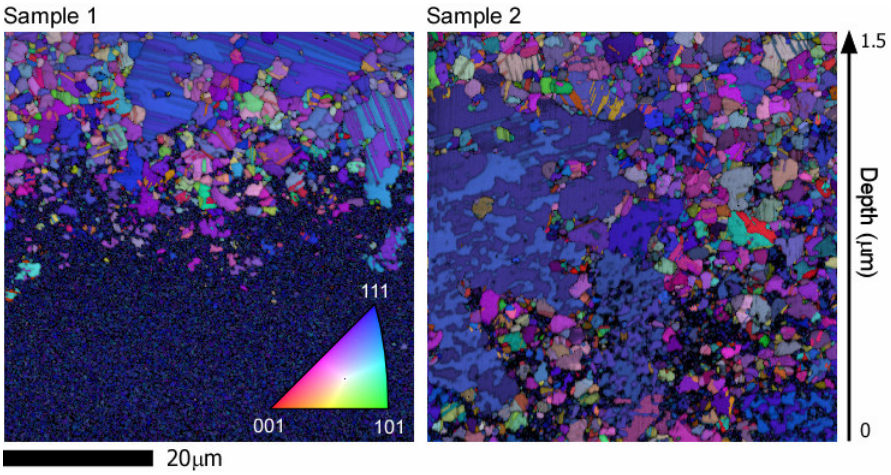

Figure 5 - Combined Image Quality and Orientation Map (Surface Normal Direction) from Samples 1 and 2.

The OIM data was also collected using the FEI Quanta 3D instrument, with the electron beam used for imaging and EBSD pattern formation. An electron beam energy of 20kV was used, with an approximate incident beam current of 4nA. Data was collected using an EDAX Hikari EBSD detector and OIM Data Collection software version 5.31. To minimize the risk of charging and drifting artifacts, data was collected at a rate of 190 indexed EBSD patterns per second. From each sample, EBSD patterns were collected from a 55µm x 55µm area with a step size of 100nm between measurements over a hexagonal collection grid for a collection time of approximately 30 minutes per sample.

In Figure 5, the images shown are combined Image Quality (IQ) and Orientation maps. The image quality value is calculated from the EBSD pattern, as is a measurement of, among other things, the quality of the diffracting crystal lattice at each measurement point [17]. In these images the IQ value is mapped as a grayscale value, with lower quality points shaded darker

than higher quality points. The orientation at each point, relative to the sample normal direction (ND), is then plotted in color, according to the stereographic triangle key shown. Preferred orientations often occur during thin film deposition due to energy minimization. Two key microstructural features are observed. First, the primary orientation present in both samples is a (111) surface normal orientation. Second, a variation in microstructure as a function of film depth is also present. This is particularly pronounced in Sample 1, but also observed in Sample 2. This bimodal microstructure has a lower image quality component located closer to the film surface and a higher quality component deeper within the film.

OIM can also be used to quantitatively determine grain size and shape, by grouping together adjacent pixel measurements with similar crystallographic orientations. Grain determination results are shown in Figure 6, where a grain tolerance angle of 5º was used for pixel grouping. In these images, determined grains are randomly colored, with no two adjacent grains colored similarly, in order to display grain size and morphology. Grain size distributions can help identify film growth mechanisms [18]. Additionally twin boundaries can be either included or excluded from the pixel grouping routine. This functionality might be significant, as attempts to correlate film grain size with efficiency show poor correlation [19]. However with different grain boundary types exhibiting different electrical performance, efficiency correlations may require grain size calculations based only on a subset of specific grain boundaries. The grain maps also show that the lower image quality regions observed in Figure 4 correspond to a smaller grain size and that these smaller grains tend to occur closer to the sample surface. The ability to measure grain shape may also be useful, as current transport path through grains and grain boundary networks can be images through cross-sectional view of the films.

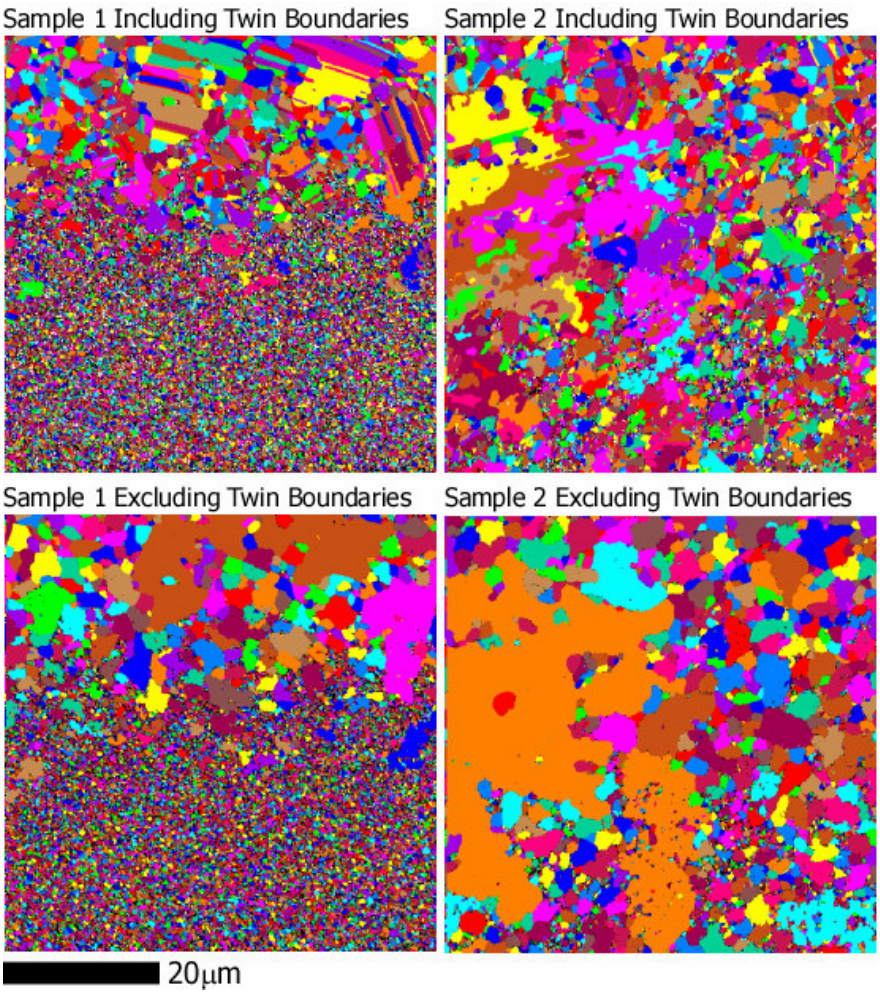

Figure 6 - Grain maps (randomly colored) of samples 1 and 2 including and excluding twin boundaries in the pixel grouping.

Different grain boundary types can be determined and displayed with OIM, as shown in Figure 7. Here random grain boundaries with a misorientation between 5º and 15º are drawn as green lines, while random grain boundaries with misorientations greater than 15º are drawn as white line. Twin boundaries (CSL Σ3 boundaries) are drawn as red lines, and second order twins (CSL Σ9 boundaries) are drawn as blue lines. Other CSL boundaries (Σ5 – Σ29) are drawn as yellow lines. It is also possible to identify and differentiate coherent and non-coherent twin boundaries [20, 21]. These different grain boundary types are expected to have different electrical characteristics and properties. With the capability to measure and quantify these grain boundary types, it becomes feasible to try and correlate these boundary structures with their electrical properties.

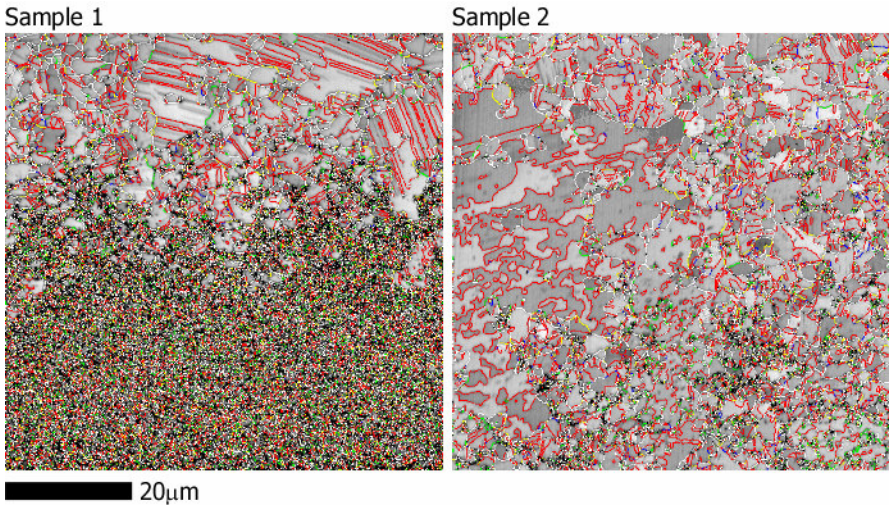

Figure 7 - Grain boundary maps with misorientations between 5º and 15º colored green, misorientations greater than 15º colored white, CSL Σ3 boundaries colored red, 2nd order Σ twin boundaries colored blue, and other CSL boundaries colored yellow.

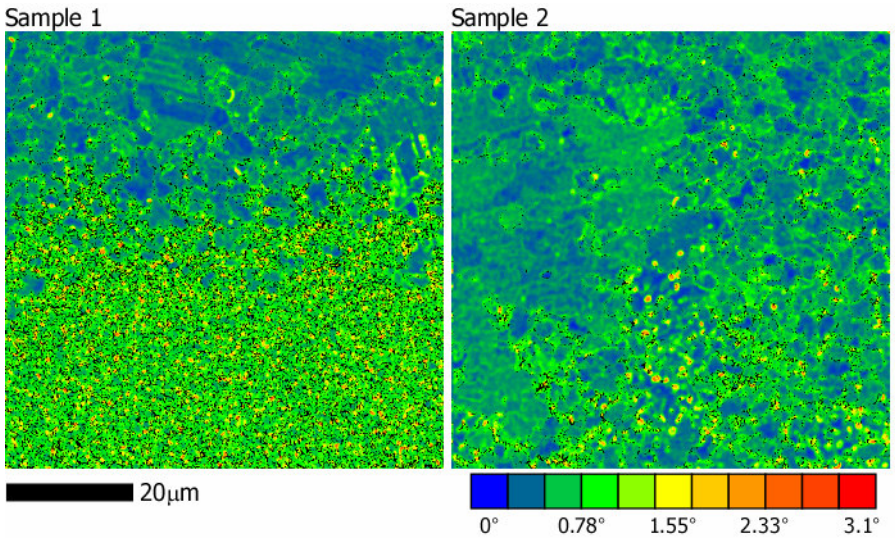

Figure 8 - Local Orientation Spread Maps based on 3rd nearest neighbor kernel.

The grain boundary maps display boundaries with misorientations greater than 5º. Boundaries with misorientations below this threshold are typically considered sub-grain boundaries. While these could also be shown in a similar manner, OIM provides alternative methods of examining this type of internal defect structure within grains. One such manner, the Local Orientation Spread, is shown in Figure 8. In this approach the misorientation between each point in a specified kernel (3rd nearest neighbors in this case – as shown in Figure 9) and all other points in the kernel is calculated, while ignoring misorientations greater than the specified threshold (5º). The average misorientation value for the kernel is then determined and assigned to the center point. This

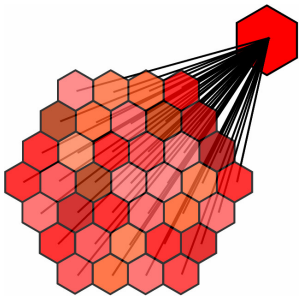

Figure 9 – A schematic of the method used to calculate the orientation spread for a 3rd nearest neighbor kernel. The misorientation between each point in the kernel with the average orientation is calculated. The average of these misorientations is then assigned to the center point of the kernel.

calculation is done for a kernel based on each point within the map. This approach is similar to calculating the average orientation of each kernel and calculating the deviation from the average for each point within that kernel but avoids problems of points near grain boundaries. It also helps to minimize the effect of measurement step size. For these samples, points within the smaller grains generally have a greater local orientation spread than those within the larger grains. To verify that this observation is not due to artifacts from measurements close to grain boundaries, where EBSD patterns may overlap, values calculated while ignoring points adjacent to grain boundaries were taken. Additionally OIM maps were collected with smaller measurements step sizes (10nm and 20nm). Both approaches confirmed that the small grains had larger orientation spread values.

The OIM data provides some interesting insight into the effects of the $CdCl_2$ treatment on these CdTe films. The bimodal distribution of image quality, grain size, and local orientation spread suggest that these films have been partially recrystallized, and that Sample 2 has recrystallized more than Sample 1. This correlates well with the difference in treatment time, 5 minutes (sample 1) versus 30 minutes (Sample 2). The smaller grains are assumed to be non-recrystallized, although examination of as-deposited non-treated samples could confirm this and also indicate whether any recovery or has occurred. The lower image quality values and higher local orientation spread indicate a larger amount of stored energy which would serve as a driving force for further recrystallization. The larger recrystallized grains have a lower orientation spread and a higher number of twin boundaries, which suggest twinning is an important active mechanism during recrystallization and grain growth. The position of more recrystallized grains deeper within the film suggest that recrystallization starts nearer the CdS/CdTe interface, where interfacial strain energies are higher due to the atomic mismatch between the hexagonal CdS and cubic CdTe phases and differences in thermal expansion coefficients. This is in contrast to previous reports of recrystallization starting at the CdTe surface [22].

The ability to measure so many microstructural features makes OIM a powerful analytical tool. Additionally OIM can divide the total data into subsets based on any number of metrics. For example, the data from these samples was divided by grain size into two sets: grains smaller than 1 micron (diameter), and grains larger than one micron (diameter). (111) pole figures from each of these two subsets is shown in Figure 10. The smaller non-recrystallized grains have a strong (111) fiber texture while the larger grains exhibit weaker textures that are dominated by a few larger grains within the analysis area. Typically 1,000 to 10,000 grains should be measured to accurately characterize a preferred orientation [23]. The number of grains within each subset is given in Table 1 along with other measurements. It should be notes that although there are 1,000+ grains measured for each subset, the grains here are calculated while included Twin boundaries during the pixel grouping calculations.

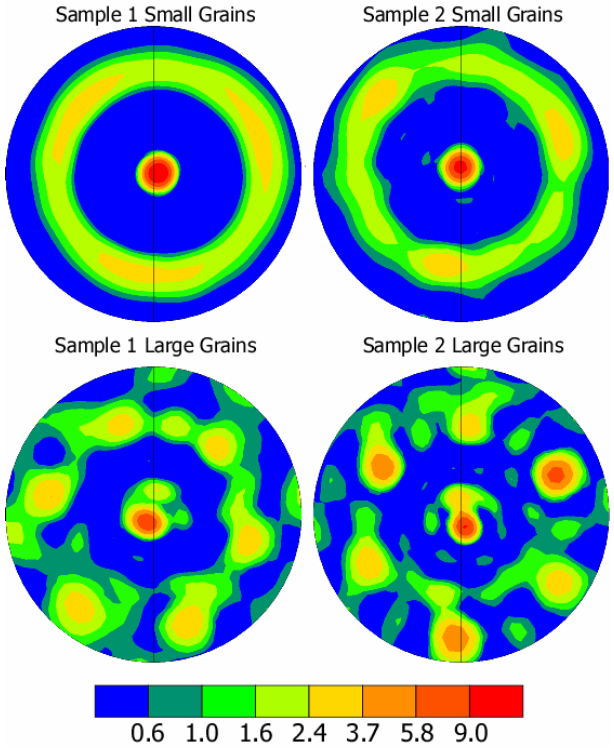

Figure 10 - (111) Pole Figures for small grains (< 1µm) and large grains (> 1µm).

The data in Table 1 allows better quantification of the data observed in the OIM images. The recrystallized grains show a drop in (111) orientation. In this case, the percentage of (111) orientation is defined as any pixel within 15º of the exact (111) alignment with the surface normal direction. Note in Figure 10 that in each subset, the maximum intensity of the (111) peak does not exactly coincide with the center of the pole figure. While part of this measurement may correspond to a slight offset in sample positioning, there is also a shift in the peak positions between the small and large grain subsets, indicating a real change. This information may help indicate if the recrystallization is occurring through a preferred nucleation or preferred growth regime. The larger grains also have an increased fraction of Σ3 twin boundaries. The loss of (111) texture with CdCl2 treatment has been reported previously [24]. These results suggest the reduction of (111) orientation may be occurring through the introduction of new twin-related orientations [25]. The fraction of other CSL boundary types is constant, indicating no preferential development of these boundary types during recrystallization. Finally the local orientation spread values are significantly higher for the smaller non-recrystallized grain.

Table 1

OIM Measurement Type	Small Grains		Large Grains	
	Sample 1	Sample 2	Sample 1	Sample 2
Number of Grains	19,370	3,014	1,083	2,488
Percentage (111) Orientation	87.4	64.4	53.9	54.9
Image Quality (Average)	689	1095	1300	1319
Percentage Twin (Σ3) Boundaries	21.2	33.3	41.9	61.1
Percentages Other CSL Boundaries	6.1	6.3	5.2	5.2
Local Orientation Spread Average (º)	0.87	0.75	0.44	0.49

This case study is designed to give an idea of the types of data that can be acquired with OIM, and how it can be used to understand the microstructural evolution that has occurred during the $CdCl_2$ activation treatment. However OIM can be used to evaluate the microstructure at almost any point during the film and device fabrication. OIM can be used to measure the texture and grain boundary character of stainless steel and molybdenum substrates used for CIGS devices, and understand how preferred orientations in the CIGS film can develop[26]. The deposition method and related variables (source and substrate temperatures, gas temperature, pressure, composition, and flow rate, deposition rate, final film thickness, etc.) can also influence the final microstructural character. As noted earlier, if improved performance can be correlated to specific microstructural features such as grain boundary type fractions, grain size (defined in a variety of ways), or film texture, it becomes possible to use OIM as a tool to measure microstructure as a function of processing, understand observed performance and efficiency behavior, and to optimize performance based on these measurements. This concept is at the core of materials science, and when in relation to grain boundaries as been termed grain boundary engineering. These concepts have been applied to other thin film materials previously [27, 28] and may help improve the efficiency of photovoltaic thin films as well.

Conclusions

- As polycrystalline CdTe and CIGS thin film photovoltaics exhibit higher efficiencies than their single crystal equivalents, the grain boundaries present must play a determining role in this improved performance.
- Not all grain boundaries exhibit equivalent behavior. Relative changes in electrical properties among different grain boundary types have been observed. Some of these changes have been correlated to crystallographic structure.
- Orientation Imaging Microscopy (OIM) is a microanalytical characterization technique well-suited to measuring the grain boundary character, preferred orientation, grain size, and strain of these photovoltaic materials.
- These measurements can provide the missing link for understanding the relationship between film processing (deposition, activation treatments, etc) and photovoltaic performance (efficiency, fill factor, etc).

Acknowledgements

The authors acknowledge Helio Moutinho from NREL for providing the $CdCl_2$ treated CdTe films and Professor David Field from Washington State University for valuable discussions about grain boundary engineering in thin films.

Selected References

1. Visoly-Fisher, I., et al., *Understanding the Beneficial Role of Grain Boundaries in Polycrystalline Solar Cells from Single-Grain-Boundary Scanning Probe Microscopy*. Advanced Functional Materials, 2006. **16**(5): p. 649-660.

2. Visoly-Fisher, I., S.R. Cohen, and D. Cahen, *Direct Evidence for Grain-Boundary Depletion in Polycrystalline CdTe from Nanoscale-Resolved Measurements*. Applied Physics Letters, 2003. **82**(4): p. 556-558.

3. Sadewasser, S., et al., *High-Resolution Work Function Imaging of Single Grains of Semiconductor Surfaces*. Applied Physics Letters, 2002. **80**(16): p. 2979-81.

4. Baier, N., et al. *EBIC and IBIC Imaging on Polyerystalline CdTe*. Nuclear Instruments & Methods in Physics Research A, 2007 **576**: p. 5-9.

5. Abou-Ras, D., et al., *Grain-Boundary Types in Chalcopyrite-Type Thin Films and their Correlations with Film Texture and Electrical Properties*. Thin Solid Films, 2009. **517**(7): p. 2545-2549.

6. Marron, D.F., et al., *Electrical Activity at Grain Boundaries of Cu(In,Ga)Se2 Thin Films.* Physical Review B, 2005. **71**(3): p. 033306-1.

7. Kronberg, M.L.a.W., F.H., *Secondary Recrystallization in Copper.* Trans. Metall. Soc. A.I.M.E., 1949. **185**: p. 501.

8. Durose, K. *On Coincidence Site Lattice Modelling of Twins in the Sphalerite and Chalcopyrite Structures*. Materials Research Society Symposium Proceedings Vol. 1012, 2007. Warrendale, PA, USA: Materials Research Society.

9. Contreras, M.A., et al., *Progress Toward 20% Efficiency in Cu(In,Ga)Se2 Polycrystalline Thin-Film Solar Cells.* Progress in Photovoltaics: Research and Applications, 1999. **7**(4): p. 311-16.

10. Fraas, L.M., *Basic Grain-Boundary Effects in Polycrystalline Heterostructure Solar Cells*. Journal of Applied Physics, 1978. **49**(2): p. 871-875.

11. Meyers, P.V. *First Solar Polycrystalline CdTe Thin Film PV*. 2006. Piscataway, NJ, USA: IEEE.

12. Demtsu, S.H. and J.R. Sites. *Quantification of Losses in Thin-Film CdS/CdTe Solar Cells*. 2005. Piscataway, NJ, USA: IEEE.

13. Moutinho, H.R., et al., *Electron Backscatter Diffraction of CdTe Thin Films: Effects of CdCl2 Treatment.* Journal of Vacuum Science & Technology A, 2008. **26**(4): p. 1068-73.

14. Abou-Ras, D., et al., *On the Capability of Revealing the Pseudosymmetry of the Chalcopyrite-Type Crystal Structure*. Crystal Research and Technology, 2008. **43**(3): p. 234-9.

15. Yanfa, Y., et al., *Understanding the Defect Physics in Polycrystalline Photovoltaic Materials.* Physica B: Physics of Condensed Matter, 2007. **401-402**: p. 25-32.

16. Al-Jassim, M.M., et al. *The Morphology, Microstructure and Luminescent Properties of CdS/CdTe Thin Film Solar Cells*. 1993. New York, NY, USA: IEEE.

17. Wright, S.I. and M.M. Nowell, *EBSD Image Quality Mapping.* Microscopy and Microanalysis, 2006. **12**: p. 72-84.

18. Abou-Ras, D., S. Schorr, and H.W. Schock, *Grain-Size Distributions and Grain Boundaries of Chalcopyrite-Type Thin Films.* Journal of Applied Crystallography, 2007. **40**: p. 841-848.

19. Eisenbarth, T., et al., *Origin of Defects in* $CuIn_{1-x}Ga_xSe_2$ *Solar Cells with Varied Ga Content*. Thin Solid Films, 2009. **517**: p. 2244-2247.

20. Wright, S.I., *Investigation of Coincident Site Lattice (CSL) Boundary Criteria in Cu Thin Films*. Journal of Electronic Materials, 2002. **31**(1): p. 50-54.

21. Wright, S.I. and R.J. Larsen, *Extracting Twins from Orientation Imaging Microscopy Scan Data.* Journal of Microscopy, 2002. **205**(3): p. 245-252.

22. Terheggen, M., et al., *Structural and Chemical Interface Characterization of CdTe Solar Cells by Transmission Electron Microscopy*. Thin Solid Films, 2003. **431-432**: p. 262-266.

23. Wright, S.I. and M.M. Nowell, *A Comparison of Texture Measurements via EBSD and X-Ray*, in Proceedings of the 15th International Conference on Textures of Materials, A.D. Rollett, Editor. 2008, The American Ceramic Society and TMS. CD.

24. Romeo, A., et al., *Study of CSS- and HVE-CdTe by Different Recrystallization Processes.* Thin Solid Films, 2009. **517**(7): p. 2132-2135.

25. Abou-Ras, D. and K. Pantleon, *The Impact of Twinning on the Local Texture of Chalcopyrite-Type Thin Films.* Physica Status Solidi (RRL), 2007. **1**(5): p. 187-189.

26. Contreras, M.A., et al. *Texture Manipulation of CuInSe2 Thin Films*. Thin Solid Films, 2000. **361-362**: p.167-171.

27. Field, D.P., R.C. Eames, and T.M. Lillo, *The Role of Shear Stress in the Formation of Annealing Twin Boundaries in Copper.* Scripta Materialia, 2006. **54**(6): p. 983-986.

28. Park, N.-J. and D.P. Field, *Predicting Thickness Dependent Twin Boundary Formation in Sputtered Cu Films.* Scripta Materialia, 2006. **54**(6): p. 999-1003.